

Lymphocyte Infiltration Determines the Hypoxia-Dependent Response to Definitive Chemoradiation in Head-and-Neck Cancer – Results from a Prospective Imaging Trial

Nils H. Nicolay^{1,2}, Alexander Rühle^{1,2}, Nicole Wiedenmann^{1,2}, Gabriele Niedermann^{1,2}, Michael Mix³,

Wolfgang A. Weber⁴, Dimos Baltas^{1,2}, Martin Werner^{2,5}, Gian Kayser^{2,5#}, Anca-L. Grosu^{1,2#}

#shared senior authorship

¹Department of Radiation Oncology, Medical Center–University of Freiburg, Faculty of Medicine, University of Freiburg, Freiburg, Germany

²German Cancer Consortium (DKTK), Partner Site Freiburg and German Cancer Research Center (DKFZ), Heidelberg, Germany

³Department of Nuclear Medicine, Medical Center–University of Freiburg, Faculty of Medicine, University of Freiburg, Freiburg, Germany

⁴Department of Nuclear Medicine, Technical University of Munich, Munich, Germany

⁵Institute of Surgical Pathology, Department of Pathology, Medical Center–University of Freiburg, Faculty of Medicine, University of Freiburg, Freiburg, Germany

Corresponding author:

Nils H. Nicolay, M.D., Ph.D.

Medical Center–University of Freiburg, Department of Radiation Oncology

Robert-Koch-Str. 3

79106 Freiburg, Germany

nils.nicolay@uniklinik-freiburg.de

+49-761-270-95200

Short running title: Hypoxia and Immune System in HNSCC

Word count: 4988 words

The trial was funded by the German Cancer Consortium (DKTK) and registered with the German Clinical Trial Register (DRKS00003830).

ABSTRACT

Tumor hypoxia in head-and-neck squamous cell carcinoma (HNSCC) leads to an immunosuppressive microenvironment and reduces the response to radiotherapy. In this prospective imaging trial, we investigated potential interactions between functional hypoxia imaging and infiltrating lymphocyte levels as a potential predictor for treatment response in HNSCC patients.

Methods

49 patients receiving definitive chemoradiation for locally advanced HNSCCs underwent pre-therapeutic biopsies and peri-therapeutic hypoxia imaging using Fluorine-18-misonidazole (¹⁸F-FMISO) PET at weeks 0, 2 and 5 during chemoradiation. Hematoxylin-eosin and immunohistochemical stainings for tumor-infiltrating lymphocytes, tissue-based hypoxia and microvascular markers were analyzed and correlated with the longitudinal hypoxia dynamics and patient outcomes.

Results

High levels of tumor-infiltrating total lymphocytes correlated with superior loco-regional control (LCR) (HR=0.279, $p=0.011$) and progression-free survival (PFS) (HR=0.276, $p=0.006$). Similarly, early resolution of ¹⁸F-FMISO PET-detected tumor hypoxia quantified by ¹⁸F-FMISO dynamics between weeks 0 and 2 of chemoradiation was associated with improved LRC (HR=0.321, $p=0.015$) and PFS (HR=0.402, $p=0.043$). Outcomes in the favorable early hypoxia resolution subgroup significantly depended on infiltrating lymphocyte counts with patients showing both early hypoxia response and high lymphocyte infiltration levels exhibiting significantly improved LRC (HR=0.259, $p=0.036$) and PFS (HR=0.242, $p=0.017$) compared to patients with early hypoxia response but low lymphocyte counts. These patients exhibited comparable oncological results to patients with no hypoxia response within the first 2 weeks of chemoradiation.

Conclusion

This analysis established a clinical hypoxia-immune score that predicted treatment responses and outcomes in HNSCC patients undergoing chemoradiation which may help to devise novel concepts for biology-driven personalization of chemoradiation.

Key words: head-and-neck cancer, hypoxia, FMISO PET, chemoradiation, immune system

INTRODUCTION

Head-and-neck squamous cell cancers (HNSCCs) are common malignancies with 650,000 new diagnoses each year (1). Radiotherapy, often combined with systemic therapies, constitutes a standard treatment for HNSCC, and 5-year overall survival ranges between 40 and 70% depending on tumor stage and localization (2).

Tumor-associated hypoxia is a key factor influencing treatment outcomes of HNSCC patients, and hypoxia increases resistance of HNSCCs to ionizing radiation both *in vitro* and clinically (3-6). Different methods of detecting and monitoring tumor-associated hypoxia during radiotherapy have been investigated, including histopathological analyses, blood- and tissue-based biomarkers, and different imaging modalities (7-13). Fluorine-18 misonidazole (¹⁸F-FMISO) tracer uptake corresponds well with invasive tissue oxygen measurements, and positron emission tomography (PET) using ¹⁸F-FMISO has been established as the imaging gold standard for longitudinal non-invasive hypoxia monitoring (14). Several analyses have investigated the role of hypoxia dynamics during radiotherapy, and early hypoxia dynamics rather than individual measurements seem to predict treatment response (15,16).

Similarly, HNSCC immunogenicity has been previously investigated, and tumor infiltration by lymphocytes and individual lymphocyte subpopulations has been linked to radiotherapy response and patient outcomes (17). Pre-treatment biopsies enable baseline histopathological lymphocyte analyses, but to date, no non-invasive procedures for monitoring HNSCC immune dynamics during radiotherapy are available.

There is increasing evidence for an interplay between tumor-associated hypoxia and the immune response within a tumor's microenvironment, but clinical data are lacking (18). For instance, most studies showed that hypoxia promotes M2 polarization of macrophages, supports the pro-tumorigenic effects of myeloid-derived suppressor cells and induces the differentiation of CD4-positive T lymphocytes into immunosuppressive regulatory T cells (19). While an in-depth understanding of the interplay between lymphocyte infiltration and hypoxia dynamics may be crucial to predict radiation responses and to personalize treatment concepts, no data are available yet.

This prospective trial investigated the predictive roles of tumor-associated hypoxia and tumor-infiltrating lymphocytes both individually and regarding their interplay in a homogenous cohort of HNSCC patients undergoing chemoradiation.

MATERIAL AND METHODS

Patient Treatment

This trial was registered with the German Clinical Trial Register (DRKS00003830) and was approved in advance by the Independent Ethics Committee of the University of Freiburg (reference no. 479/12). 49 patients with histologically confirmed locally advanced HNSCC undergoing definitive chemoradiation were enrolled in this prospective trial. Exclusion criteria were disorders interfering with the patients' compliance to adhere to the study protocol (e.g. dementia), a Karnofsky performance status $\leq 70\%$, claustrophobia and other magnetic resonance imaging (MRI) contraindications, previous malignancies, prior HNSCC resection, distant metastases and pregnancy. Detailed patient characteristics are summarized in table 1. Patients received definitive chemoradiation using intensity-modulated radiotherapy to a cumulative dose of 70 Gy in 35 fractions. Concomitant systemic treatment was administered with up to 3 cycles of cisplatin (100 mg/m^2 body surface area in weeks 1, 4, 7). Loco-regional control (LRC), progression-free survival (PFS) and overall survival (OS) were calculated from the initiation of chemoradiation. All patients provided written informed consent, and all aspects of this trial were performed in accordance with the Declaration of Helsinki.

Imaging

All patients underwent initial computed tomography (CT) and MRI scans as well as PET imaging with ^{18}F -fluorodeoxyglucose (^{18}F -FDG) and ^{18}F -FMISO tracers prior to treatment. Further ^{18}F -FMISO PET imaging was carried out in weeks 2 and 5 during chemoradiation (figure 1). PET imaging for the first 15 patients was performed on an ECAT EXACT 921 PET scanner (Siemens, Erlangen, Germany) and for the consecutive patients on a Gemini TrueFlight PET/CT scanner (Philips, Hamburg, Germany). ^{18}F -FMISO

was administered at 3.7 MBq/kg to a maximum activity of 370 MBq; hypoxia imaging was performed in radiotherapy position using a thermoplastic head immobilization mask at 150 minutes after tracer administration (3 frames at 10 minutes each, followed by a transmission scan for 5 minutes). PET images were co-registered to the corresponding planning CTs, and quantitative analyses were performed using a sum of 3 attenuation-corrected frames as described previously (16).

Gross tumor volumes (GTVs) were manually delineated using the ¹⁸F-FDG-PET-MRI co-registered images using a PET threshold of 40% of the maximum standardized uptake value (SUV) within the tumor (16). All GTVs were individually cross-validated with the co-registered planning CTs by 2 experienced physicians. Hypoxic subvolumes were defined as all voxels within the GTV with a ratio of ¹⁸F-FMISO SUV to mean SUV in the contralateral sternocleidomastoideus muscles above 1.4. The ratio was based on published thresholds and has previously been validated in this trial cohort (16,20).

Imaging parameters investigated in this analysis comprised the ¹⁸F-FMISO uptake-defined hypoxic subvolumes and the SUV index (normalized ¹⁸F-FMISO SUV_{max}) as the ratio between the maximum tumor SUV and the mean SUV in the contralateral sternocleidomastoid muscle at weeks 0, 2 and 5. Hypoxia dynamics during the course of treatment (Δ SUV index) were quantified by subtracting the SUV index at baseline from the values of weeks 2 or 5 and calculating the percentage of change.

Immunohistochemistry

Pre-treatment biopsies were carried out for all patients to confirm diagnosis. Tumor samples were formalin-fixed and embedded in paraffin according to institutional histopathology protocols. Tumors were sectioned to 2 μ m and mounted on coated glass slides before deparaffinization and rehydration through descending graded ethanol concentrations. Antigens were retrieved by heat induction, and endogenous peroxidase activity was blocked using H₂O₂. Antigen complexes were visualized by a mouse linker (DAKO) and Envision Flex Kit using horseradish peroxidase-diaminobenzidine (HRP-DAB) reaction (DAKO) as chromogen. Details of primary antibodies and antigen retrieval are outlined in supplementary table 1.

Hypoxia markers CAIX and HIF1 α were assessed semi-quantitatively by the H-score. Staining intensity (0=no staining, 1=weak, 2=moderate, 3=strong) was assessed in all viable tumor cells, and the H-score (range 0-300) was quantified as the sum of the tumor cell percentages of the different staining intensities multiplied by their specific intensity scores.

Microvessel density was investigated by CD34 staining and divided into 3 categories: 1—only larger vessels in the stroma, no contact to tumor cells; 2—smaller vessels in the stroma with contact to tumor cells, no vessels intermingled in the tumor-stroma border; 3—small vessels intermingling with tumor cells at the tumor-stroma border.

Lymphocyte infiltration was quantified per high-power field (HPF) and was dichotomized into low (<100 cells/HPF) and high infiltration levels (>100 cells/HPF). Lymphocyte scoring was performed both for the intraepithelial and stromal compartments. While total lymphocyte scoring was based on hematoxylin-eosin stainings, quantification of total T lymphocytes, CD4-positive and CD8-positive T lymphocytes depended on the immunohistochemical stainings for CD3, CD4 and CD8, respectively. Blinded samples were used for histological analyses, and one section of the same paraffin block was analyzed for each marker.

Statistical Analyses

Statistical analyses were carried out to assess potential correlations between individual tissue-based variables and between tumor tissue variables and imaging variables. Statistical significance of variable pairs was tested by the Pearson's product-moment correlation. Clinical outcome parameters were investigated using the Kaplan-Meier method, and correlations between individual tumor tissue variables and clinical outcome parameters were analyzed using the log-rank test and the Cox proportional hazards model. Hazard ratios (HR) are indicated together with the corresponding 95% confidence interval, and statistical significance was assumed for $p<0.05$.

RESULTS

High Levels of Tumor-Infiltrating Lymphocytes are Associated with Improved LRC and Survival

High numbers of total infiltrating total lymphocytes correlated with a significantly improved LRC (HR=0.279 [0.104-0.748], $p=0.011$) and PFS (HR=0.276 [0.110-0.690], $p=0.006$) (figure 2). Also for the subgroup of HPV-negative HNSCC patients, LRC (HR=0.296 [0.104-0.842], $p=0.022$) and PFS (HR=0.250 [0.089-0.700], $p=0.008$) were superior for patients with high tumor-infiltrating lymphocyte levels (supplementary figure 1).

Similarly, high levels of CD3-positive T lymphocytes revealed a trend towards higher LRC (HR=0.370 [0.126-1.082], $p=0.058$) and significantly improved PFS (HR=0.320 [0.118-0.866], $p=0.019$), while OS was increased with borderline-significance (HR=0.260 [0.067-1.006], $p=0.051$) (supplementary figure 2). For HPV-negative HNSCCs, higher levels of tumor-infiltrating CD3-positive T lymphocytes led to a trend towards increased PFS (HR=0.361 [0.126-1.040], $p=0.059$) but not LRC (HR=0.468 [0.158-1.387], $p=0.171$). Neither LRC (HR=2.094 [0.679-6.456], $p=0.215$) nor PFS (HR=2.389 [0.839-6.806], $p=0.117$) differed between patients with high and low numbers of CD4-positive T lymphocytes (supplementary figure 3), and CD8-positive lymphocyte levels also did not correlate with LRC (HR=0.578 [0.128-2.609], $p=0.448$), PFS (HR=0.679 [0.193-2.387], $p=0.531$) or OS (HR=0.578 [0.128-2.609], $p=0.448$) (supplementary figures 2 and 3).

Lymphocyte Infiltration does not Correlate with Tissue-Based Hypoxia Biomarkers

Pairwise correlations were performed between expression levels of immune and hypoxia biomarkers as well as p16 status using Pearson's correlation coefficient. Numbers of infiltrating lymphocyte subgroups did not correlate with the tested tissue-based hypoxia biomarkers HIF1 α or CAIX (supplementary table 2). However, strong expression of the microvascular protein CD34 as an indirect surrogate marker for tissue hypoxia corresponded with significantly increased levels of total infiltrating lymphocytes ($r=0.476$; $p=0.003$) and a trend towards high numbers of CD3-positive ($r=0.313$; $p=0.059$) and CD8-positive T lymphocytes ($r=0.275$; $p=0.099$).

Early Resolution of Tumor-Associated Hypoxia During Chemoradiation is Associated with Improved LRC and Survival

Dynamics of tumor-associated hypoxia during chemoradiation were assessed by the SUV index in weeks 0, 2 and 5 during treatment as well as differences between the different time points. 29 patients demonstrated an early decrease in their SUV indices between weeks 0 and 2, and all but one patient demonstrated a reduction in tumor-associated hypoxia between weeks 2 and 5. Early hypoxia resolution as indicated by a negative Δ SUV index between weeks 0 and 2 resulted in significantly improved LRC (HR=0.321 [0.134-0.770], $p=0.015$) and PFS (HR=0.402 [0.173-0.936], $p=0.043$) compared to an increase in hypoxia during the first two treatment weeks, but no effect on OS (HR=0.785 [0.275-2.242], $p=0.657$) (figure 3). Using the SUV index cut-off value of 1.4 in week 2, patients with no/low tumor hypoxia had considerably enhanced LRC (HR=0.314 [0.103-0.953], $p=0.041$) and PFS (HR=0.273 [0.091-0.820], $p=0.021$) (supplementary table 3). For the subgroup of HPV-negative HNSCC patients, early hypoxia response resulted in a trend towards improved LRC (HR=0.465 [0.189-1.143], $p=0.095$) and PFS (HR=0.555 [0.229-1.344], $p=0.095$) (supplementary figure 1).

High Lymphocyte Levels Determine the Response of Hypoxia-Resolving and Non-Resolving HNSCCs to Radiotherapy

To assess the individual values of lymphocyte infiltration and hypoxia dynamics as potential predictors for the response to chemoradiation, patients were divided into four groups according to their status of early hypoxia resolution and their levels of infiltrating lymphocytes at initial biopsy. Even within the group of patients that demonstrated an early resolution of tumor-associated hypoxia, infiltrating lymphocyte levels significantly determined outcomes, and patients with high numbers of total lymphocytes demonstrated superior LRC (HR=0.259 [0.072-0.926], $p=0.036$) and PFS (HR=0.242 [0.075-0.775], $p=0.017$) compared to patients with low lymphocyte counts (figure 4). Considering only the HPV-negative HNSCC patients, the favorable subgroup (negative SUV indices dynamics between weeks 0 and 2 and high tumor-infiltrating lymphocyte levels) still had significantly increased LRC (HR=0.262 [0.072-0.947], $p=0.041$)

and PFS (HR=0.202 [0.058-0.706], $p=0.012$) compared to patients displaying early hypoxia response but low lymphocyte levels.

In contrast, patients with low total infiltrating lymphocyte numbers exhibited only non-significantly improved LRC (HR=0.359 [0.080-1.615], $p=0.201$) and PFS (HR=0.462 [0.110-1.946], $p=0.313$) in case of an early hypoxia resolution compared to patients with no resolution. In turn, patients with high counts of CD3-positive T lymphocytes showed superior LRC (HR=0.246 [0.051-1.191], $p=0.054$) and PFS (HR=0.256 [0.064-1.017], $p=0.038$) within the favorable patient subgroup with an early PET-detected hypoxia response. Levels of CD4- or CD8-positive lymphocytes were not able to discriminate between outcomes for patients with an early resolution or increase in tumor-associated hypoxia (supplementary figure 4). Pairwise correlations between lymphocyte levels and tumor hypoxia during chemoradiation were conducted to reveal potential associations between immune cell infiltration and hypoxia levels; however, we did not find any significant correlations (table 2).

DISCUSSION

The increasing availability of tumor-specific biological and functional information may enable a better response prediction for radiotherapy which in turn will form the basis for developing individualized and personalized treatment concepts. Both molecular analyses and functional imaging modalities have provided novel insights into HNSCCs over the last years, but clear correlations between the tumor biology and the corresponding imaging information are largely unknown. However, these may be of great importance as an in-depth biological analysis commonly requires invasively harvested tissue samples, preventing longitudinal evaluations, while imaging enables non-invasive and repetitive monitoring and early response assessment of tumors during treatment. In this prospective imaging trial, we found that both an early hypoxia response within the first two weeks of chemoradiation and high levels of infiltrating lymphocytes resulted in improved LRC and PFS in HNSCC patients. Additionally, we demonstrated that the relevance of an early hypoxia response depended on the levels of infiltrating lymphocytes, and only patients with both hypoxia response and elevated numbers of intratumoral lymphocytes had superior LRC

and PFS, while patients with a hypoxia response but low lymphocyte counts exhibited significant deteriorations in their outcomes that were comparable to patients with no hypoxia response.

Several papers have shown that the immune pattern and especially the level of tumor-infiltrating lymphocytes correlate with the prognosis of HNSCC patients and may help to predict response to radiation treatment (17,21). For definitive chemoradiation, increased numbers of tumor-infiltrating CD3- and CD8-positive T lymphocytes corresponded with improved LRC and OS, while for adjuvant chemoradiation, only CD8-positive lymphocytes led to improved survival rates (17,21). In our study, the levels of CD3-positive but not CD8-positive T lymphocytes correlated with improved survival rates after definitive chemoradiation. The fact that we did not confirm the correlation between the levels of CD8-positive T lymphocytes and survival rates may be related to small biopsies and limited patient numbers. However, we observed increased infiltration of CD8-positive T lymphocytes in p16-positive HNSCC tumors, which is consistent with previous reports (22,23).

Tumor hypoxia is known to increase resistance to ionizing radiation, and ¹⁸F-FMISO PET imaging has been established as a standard measure to monitor hypoxia during radiotherapy (14). It has been demonstrated that LRC and survival of HNSCC patients are superior for tumors with rapid resolution of tumor-associated hypoxia during the first weeks of radiotherapy (15,16,24). Therefore, several approaches have been considered to improve oncological outcomes in HNSCC patients with reduced hypoxia resolution during chemoradiation. For instance, the DAHANCA-33 trial is currently investigating the impact of dose escalation in combination with cisplatin and the hypoxic modifier nimorazole for patients with locally advanced and hypoxic tumors (25). In another phase II-trial, dose escalation with 77 Gy delivered in 35 fractions to the hypoxic subvolumes was feasible with acceptable toxicity (24). A meta-analysis including almost 5000 patients demonstrated that hypoxia modification administered concomitantly to radiotherapy in HNSCC patients improved LRC and OS (26).

As both hypoxic modifiers and checkpoint inhibitors show activity in HNSCC and hypoxia leads to an immunosuppressive microenvironment, one may hypothesize that combination of hypoxic modifiers with checkpoint inhibitors could further improve the outcome compared to each treatment alone. Although

clinical trials combining hypoxia modification with checkpoint inhibitors are missing and no data are available for HNSCC yet, at least mouse models of prostate cancer have shown that a reduction of tumor hypoxia restores T cell infiltration and sensitizes cancer cells to checkpoint inhibitors (27).

Recently, a hypoxia-transcriptional classifier was proposed and validated, showing a potential to discriminate 3 patient subgroups with different hypoxia-immune phenotypes, namely a $\text{hypoxia}_{\text{low}}/\text{immune}_{\text{high}}$ -, a $\text{hypoxia}_{\text{high}}/\text{immune}_{\text{low}}$ - and a mixed phenotype (28). The authors demonstrated that each of the 3 subtypes exhibited distinct biologic characteristics with varying activated pathways, for which potentially effective targeted therapies exist. In this dataset, the $\text{hypoxia}_{\text{low}}/\text{immune}_{\text{high}}$ -phenotype was associated with markedly improved survival rates. In line with these data, we have now shown for the first time in a prospective clinical trial the superior survival of patients exhibiting early hypoxia resolution and high intratumoral lymphocyte infiltration.

While the exact underlying mechanism for the observed interaction are to be elucidated, we hypothesize that pre-existing lymphocyte infiltration of the tumor tissue may be required to exploit the disappearance of the immune-suppressing hypoxic microenvironment during chemoradiation. In this respect, HNSCC patients with insufficient numbers of tumor-infiltrating T lymphocytes may not be able to derive benefit from the resolving tumor hypoxia environment. In turn, the omission of the immune-suppressing hypoxic microenvironment during chemoradiation, which allows tumor-infiltrating T lymphocytes to exert their anti-tumor effects, may be an important mechanism by which radiotherapy-induced hypoxia resolution exerts its beneficial effects. As hypoxia upregulates TGF- β secretion, increases checkpoint protein expression and directly impairs T cells' anti-tumor activities, hypoxia resolution could restore T cells' anti-tumor functions (29). Combinations of hypoxia imaging and immuno-PET imaging in order to monitor T cell localization, thereby investigating the interaction between tumor hypoxia and the tumor immune microenvironment in real-time and non-invasively, could verify our hypotheses in the future (30,31). Recently, a first-in-human study showed the feasibility and safety of targeting CD8-positive T lymphocytes using the radiolabeled minibody ^{89}Zr -IAB22M2C (32). The potential advantages of functional immuno-PET imaging compared to tumor biopsies include the avoidance of invasive

procedures, the possibility for real-time measurements and the coverage of the whole tumor including distant metastases addressing the well-known heterogeneity of HNSCC. For instance, we did not observe a correlation between tumor-infiltrating lymphocyte levels and the hypoxia markers HIF1 α and CAIX, which may be related to the spatial distribution of tumor hypoxia that cannot be adequately addressed using small tissue samples.

Although being a prospective trial with comprehensive longitudinal hypoxia imaging and homogeneous treatment characteristics, our exploratory analysis has some limitations including the limited sample size; therefore, the data from our analysis require confirmation in larger prospective trials. Furthermore, we did not perform repeat biopsies during treatment due to ethical concerns, so no data are available about longitudinal correlations between imaging and histology. It is well known that tumors exhibit intratumoral heterogeneity, and therefore it needs to be noted that tumor biopsies may not be able to represent the complete tumor.

CONCLUSION

This dataset demonstrated that high pre-therapeutic tumor lymphocyte levels determine the response of HNSCC to definitive chemoradiation depending on their hypoxia dynamics: Patients with high levels of tumor-infiltrating lymphocytes combined with early hypoxia resolution assessed by ^{18}F -FMISO PET imaging had excellent LRC and PFS rates, while HNSCC patients exhibiting low tumor lymphocyte levels did not benefit from early hypoxia resolution. Our findings might help to devise novel concepts for personalized cancer treatment in particular for HNSCC patients.

DISCLOSURE

The authors declare that they have no conflict of interest.

ACKNOWLEDGEMENTS

The authors thank Andrei Bunea, Hatice Bunea and Raluca Stoian for their help with patient recruitment.

Alexander Rühle was supported by the IMM-PACT-Program for Clinician Scientists, Department of Medicine II, Medical Center–University of Freiburg and Faculty of Medicine, University of Freiburg, funded by the Deutsche Forschungsgemeinschaft (DFG, German Research Foundation)–413517907.

KEY POINTS

Question: How do intratumoral lymphocyte levels influence the favorable outcomes of HNSCC patients with early hypoxia resolution during definitive chemoradiation?

Pertinent findings: In this prospective imaging trial, patients received pre-therapeutic biopsies and longitudinal hypoxia imaging using ¹⁸F-FMISO PET at weeks 0, 2 and 5 during chemoradiation. We could show for the first time that outcomes in the favorable early hypoxia resolution subgroup were dependent on tumor-infiltrating lymphocyte levels: Patients exhibiting both early hypoxia response and high lymphocyte infiltration levels exhibited significantly improved LRC and PFS rates compared to patients with hypoxia response but low lymphocyte counts.

Implications for patient care: Understanding of the interplay between the immune system and tumor-associated hypoxia dynamics during chemoradiation may help to identify patients who might benefit from personalized treatment strategies, including dose escalation to hypoxic subvolumes or combination with hypoxia modifiers and checkpoint inhibitors.

REFERENCES

1. Bray F, Ferlay J, Soerjomataram I, Siegel RL, Torre LA, Jemal A. Global cancer statistics 2018: GLOBOCAN estimates of incidence and mortality worldwide for 36 cancers in 185 countries. *CA Cancer J Clin.* 2018;68:394-424.
2. Blanchard P, Baujat B, Holostenko V, et al. Meta-analysis of chemotherapy in head and neck cancer (MACH-NC): a comprehensive analysis by tumour site. *Radiother Oncol.* 2011;100:33-40.
3. Baumann R, Depping R, Delaperriere M, Dunst J. Targeting hypoxia to overcome radiation resistance in head & neck cancers: real challenge or clinical fairytale? *Expert Rev Anticancer Ther.* 2016;16:751-758.
4. Overgaard J, Eriksen JG, Nordmark M, Alsner J, Horsman MR. Plasma osteopontin, hypoxia, and response to the hypoxia sensitiser nimorazole in radiotherapy of head and neck cancer: results from the DAHANCA 5 randomised double-blind placebo-controlled trial. *Lancet Oncol.* 2005;6:757-764.
5. Mortensen LS, Johansen J, Kallehauge J, et al. FAZA PET/CT hypoxia imaging in patients with squamous cell carcinoma of the head and neck treated with radiotherapy: results from the DAHANCA 24 trial. *Radiother Oncol.* 2012;105:14-20.
6. Vaupel P, Thews O, Hoeckel M. Treatment resistance of solid tumors: role of hypoxia and anemia. *Med Oncol.* 2001;18:243-259.

7. Zips D, Zophel K, Abolmaali N, et al. Exploratory prospective trial of hypoxia-specific PET imaging during radiochemotherapy in patients with locally advanced head-and-neck cancer. *Radiother Oncol.* 2012;105:21-28.
8. Wiedenmann N, Bunea H, Rischke HC, et al. Effect of radiochemotherapy on T2* MRI in HNSCC and its relation to FMISO PET derived hypoxia and FDG PET. *Radiat Oncol.* 2018;13:159.
9. Grosu AL, Souvatzoglou M, Röper B, et al. Hypoxia imaging with FAZA-PET and theoretical considerations with regard to dose painting for individualization of radiotherapy in patients with head and neck cancer. *Int J Radiat Oncol Biol Phys.* 2007;69:541-551.
10. Stadler P, Feldmann HJ, Creighton C, Kau R, Molls M. Changes in tumor oxygenation during combined treatment with split-course radiotherapy and chemotherapy in patients with head and neck cancer. *Radiother Oncol.* 1998;48:157-164.
11. Kwon OJ, Park JJ, Ko GH, et al. HIF-1alpha and CA-IX as predictors of locoregional control for determining the optimal treatment modality for early-stage laryngeal carcinoma. *Head Neck.* 2015;37:505-510.
12. Wiedenmann N, Grosu AL, Buchert M, et al. The utility of multiparametric MRI to characterize hypoxic tumor subvolumes in comparison to FMISO PET/CT. Consequences for diagnosis and chemoradiation treatment planning in head and neck cancer. *Radiother Oncol.* 2020.

13. Nicolay NH, Wiedenmann N, Mix M, et al. Correlative analyses between tissue-based hypoxia biomarkers and hypoxia PET imaging in head and neck cancer patients during radiochemotherapy-results from a prospective trial. *Eur J Nucl Med Mol Imaging*. 2019.
14. Rajendran JG, Schwartz DL, O'Sullivan J, et al. Tumor hypoxia imaging with [F-18] fluoromisonidazole positron emission tomography in head and neck cancer. *Clin Cancer Res*. 2006;12:5435-5441.
15. Lock S, Perrin R, Seidlitz A, et al. Residual tumour hypoxia in head-and-neck cancer patients undergoing primary radiochemotherapy, final results of a prospective trial on repeat FMISO-PET imaging. *Radiother Oncol*. 2017;124:533-540.
16. Wiedenmann NE, Bucher S, Hentschel M, et al. Serial [18F]-fluoromisonidazole PET during radiochemotherapy for locally advanced head and neck cancer and its correlation with outcome. *Radiother Oncol*. 2015;117:113-117.
17. Balermpas P, Michel Y, Wagenblast J, et al. Tumour-infiltrating lymphocytes predict response to definitive chemoradiotherapy in head and neck cancer. *Br J Cancer*. 2014;110:501-509.
18. Noman MZ, Hasmim M, Messai Y, et al. Hypoxia: a key player in antitumor immune response. A Review in the Theme: Cellular Responses to Hypoxia. *Am J Physiol Cell Physiol*. 2015;309:C569-579.
19. Colegio OR, Chu NQ, Szabo AL, et al. Functional polarization of tumour-associated macrophages by tumour-derived lactic acid. *Nature*. 2014;513:559-563.

- 20.** Bittner MI, Wiedenmann N, Bucher S, et al. Exploratory geographical analysis of hypoxic subvolumes using 18F-MISO-PET imaging in patients with head and neck cancer in the course of primary chemoradiotherapy. *Radiother Oncol*. 2013;108:511-516.
- 21.** Balermpas P, Rodel F, Rodel C, et al. CD8+ tumour-infiltrating lymphocytes in relation to HPV status and clinical outcome in patients with head and neck cancer after postoperative chemoradiotherapy: A multicentre study of the German cancer consortium radiation oncology group (DKTK-ROG). *Int J Cancer*. 2016;138:171-181.
- 22.** Nguyen N, Bellile E, Thomas D, et al. Tumor infiltrating lymphocytes and survival in patients with head and neck squamous cell carcinoma. *Head Neck*. 2016;38:1074-1084.
- 23.** Jung AC, Guihard S, Krugell S, et al. CD8-alpha T-cell infiltration in human papillomavirus-related oropharyngeal carcinoma correlates with improved patient prognosis. *Int J Cancer*. 2013;132:E26-36.
- 24.** Welz S, Monnich D, Pfannenberg C, et al. Prognostic value of dynamic hypoxia PET in head and neck cancer: Results from a planned interim analysis of a randomized phase II hypoxia-image guided dose escalation trial. *Radiother Oncol*. 2017;124:526-532.
- 25.** Saksø M, Andersen E, Bentzen J, et al. A prospective, multicenter DAHANCA study of hyperfractionated, accelerated radiotherapy for head and neck squamous cell carcinoma. *Acta Oncol*. 2019;58:1495-1501.

- 26.** Overgaard J. Hypoxic modification of radiotherapy in squamous cell carcinoma of the head and neck--a systematic review and meta-analysis. *Radiother Oncol.* 2011;100:22-32.
- 27.** Jayaprakash P, Ai M, Liu A, et al. Targeted hypoxia reduction restores T cell infiltration and sensitizes prostate cancer to immunotherapy. *J Clin Invest.* 2018;128:5137-5149.
- 28.** Brooks JM, Menezes AN, Ibrahim M, et al. Development and Validation of a Combined Hypoxia and Immune Prognostic Classifier for Head and Neck Cancer. *Clin Cancer Res.* 2019;25:5315-5328.
- 29.** Ohta A. Oxygen-dependent regulation of immune checkpoint mechanisms. *Int Immunol.* 2018;30:335-343.
- 30.** Seo JW, Tavare R, Mahakian LM, et al. CD8(+) T-Cell Density Imaging with (64)Cu-Labeled Cys-Diabody Informs Immunotherapy Protocols. *Clin Cancer Res.* 2018;24:4976-4987.
- 31.** Tavare R, McCracken MN, Zettlitz KA, et al. Immuno-PET of Murine T Cell Reconstitution Postadoptive Stem Cell Transplantation Using Anti-CD4 and Anti-CD8 Cys-Diabodies. *J Nucl Med.* 2015;56:1258-1264.
- 32.** Pandit-Taskar N, Postow MA, Hellmann MD, et al. First-in-Humans Imaging with (89)Zr-Df-IAB22M2C Anti-CD8 Minibody in Patients with Solid Malignancies: Preliminary Pharmacokinetics, Biodistribution, and Lesion Targeting. *J Nucl Med.* 2020;61:512-519.

Figure legends

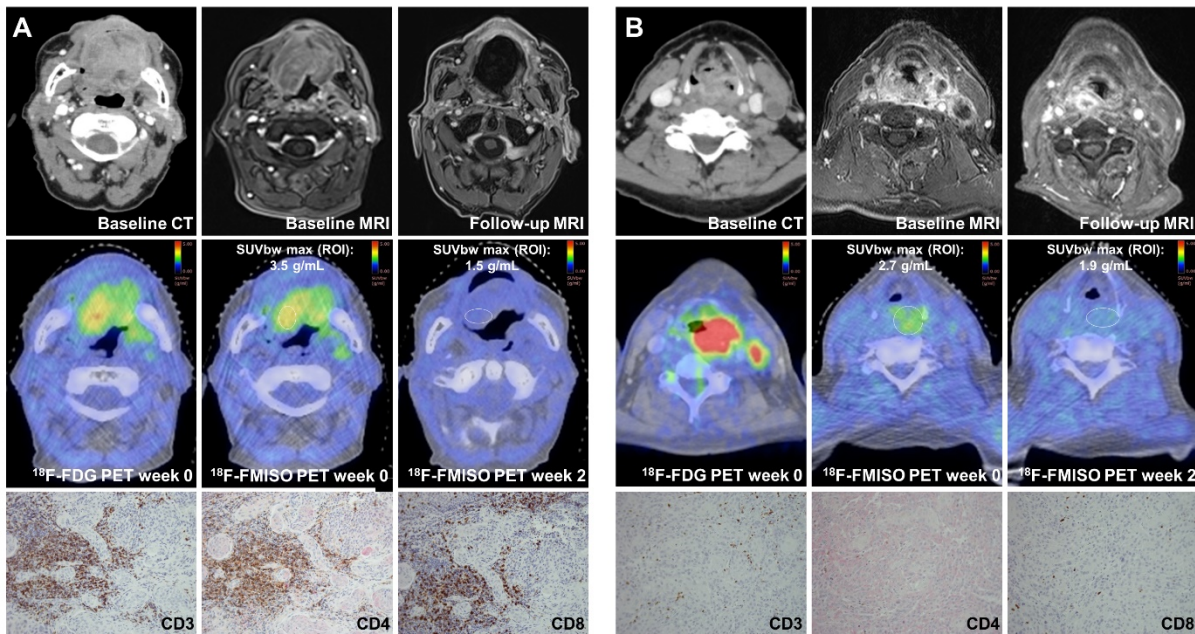


Figure 1. Lymphocyte levels and hypoxia dynamics during chemoradiation. (A) HNSCC patient with hypoxia response and high intratumoral lymphocyte levels. Pre-therapeutic CT and MRI showing an oral cavity carcinoma. Follow-up MRI imaging after 43 months showing loco-regional control. Pre-therapeutic ¹⁸F-FDG PET and ¹⁸F-FMISO PET at weeks 0 and 2; representative images of immunohistochemical stainings for CD3, CD4 and CD8.

(B) HNSCC patient with hypoxia response but low intratumoral lymphocyte levels. Pre-therapeutic CT and MRI scan showing an oro-/hypopharyngeal carcinoma. Follow-up MRI demonstrating a loco-regional relapse after 5 months. Pre-therapeutic ¹⁸F-FDG PET, ¹⁸F-FMISO PET at weeks 0 and 2; pre-therapeutic immunohistochemical staining for CD3, CD4 and CD8.

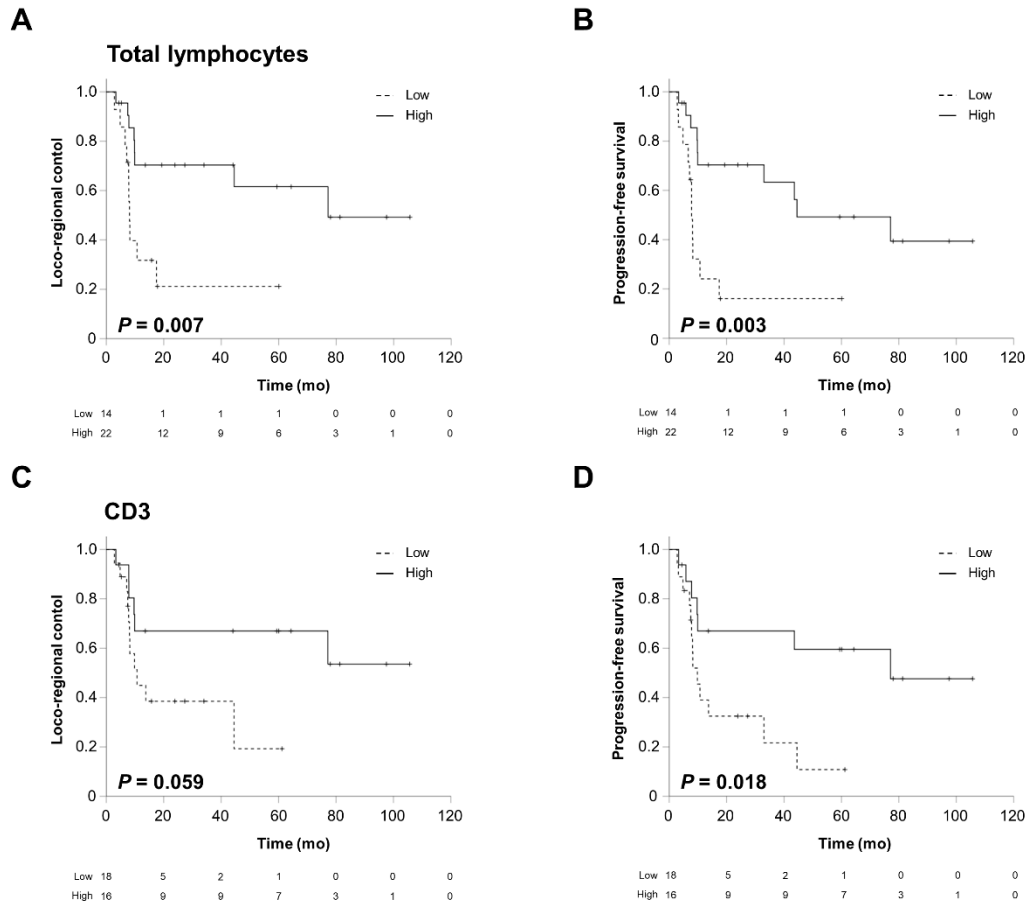


Figure 2. High lymphocyte levels correspond with increased LRC and PFS rates in HNSCC patients. LRC (A) and PFS (B) rates stratified by total tissue lymphocyte levels in tumor biopsies. LRC (C) and PFS (D) rates divided by high and low levels of CD3-positive lymphocytes.

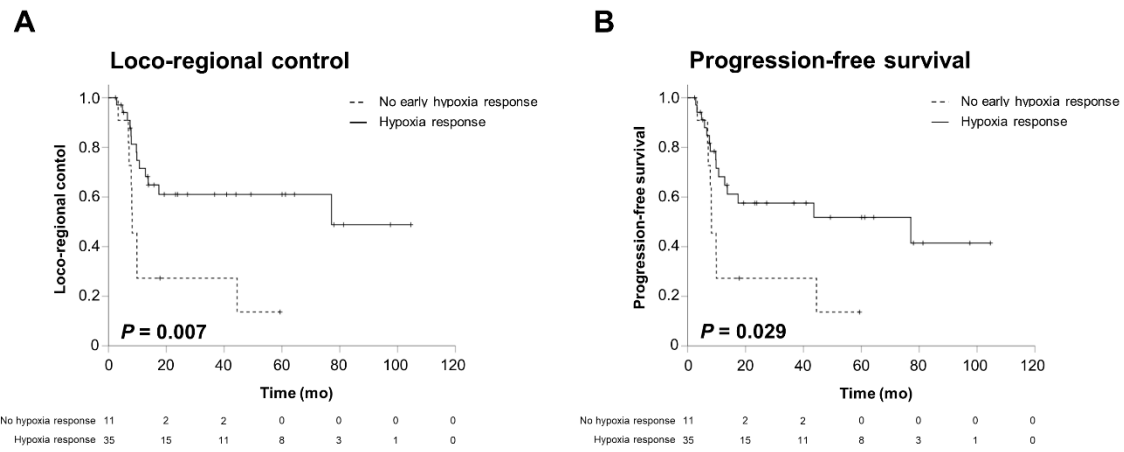


Figure 3. Early hypoxia resolution during chemoradiation is a prognosticator for improved LRC and PFS. LRC (A) and PFS (B) in HNSCC patients undergoing chemoradiation stratified by hypoxia resolution assessed by ^{18}F -FMISO PET imaging between weeks 0 and 2.

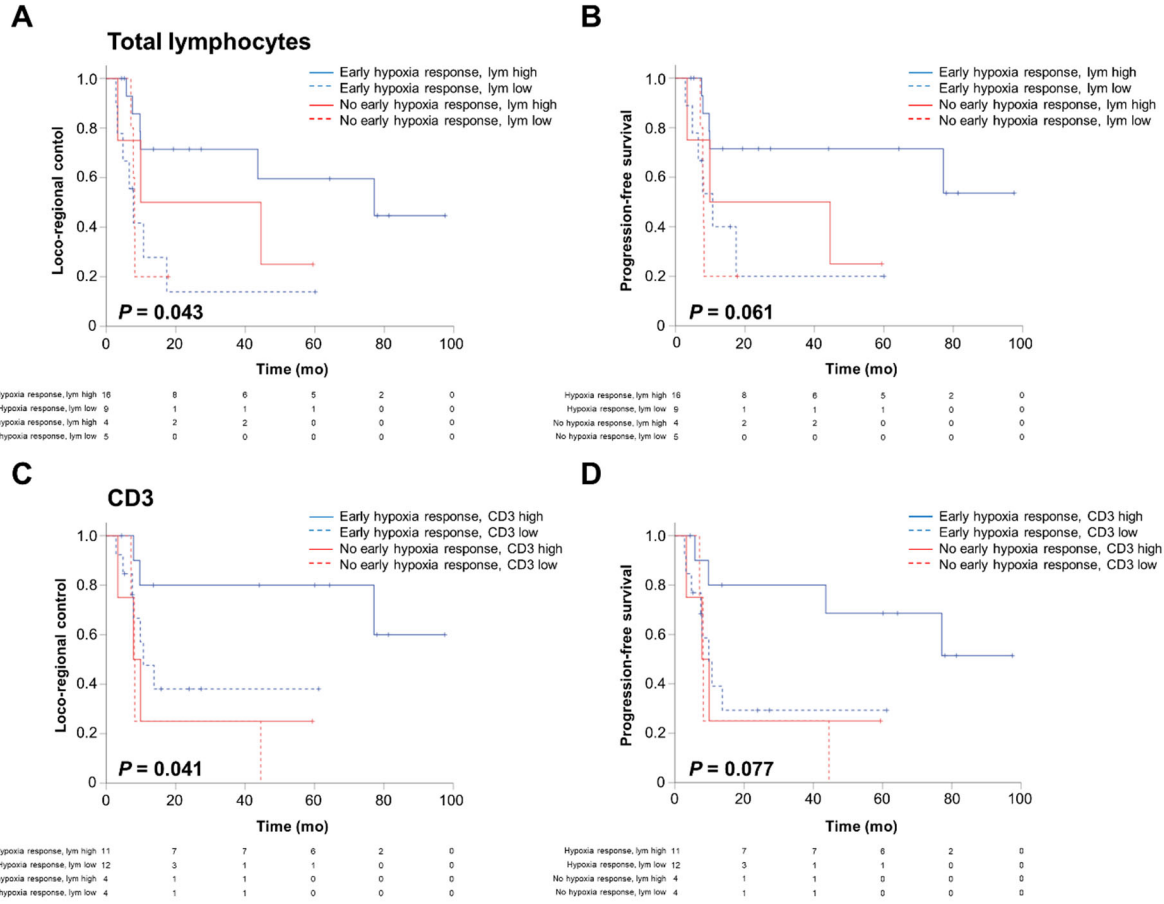


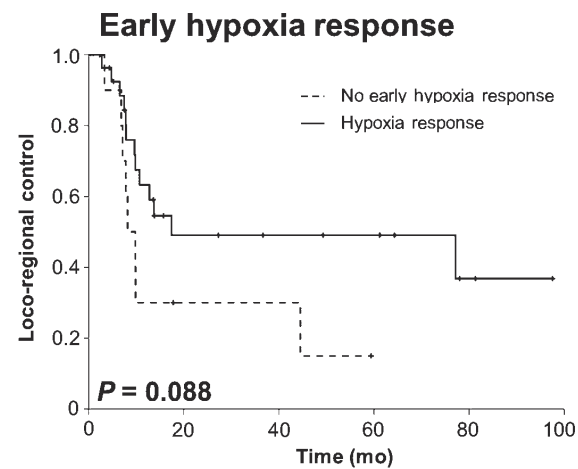
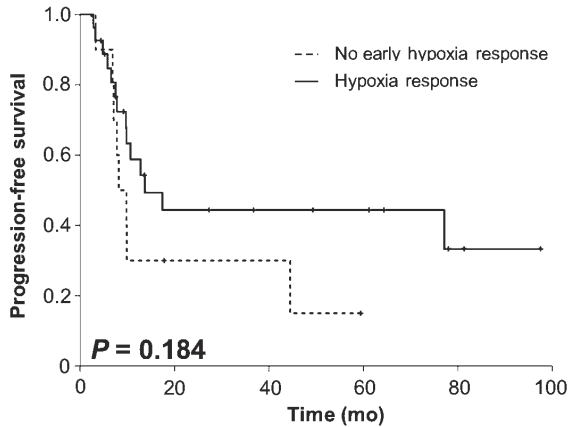
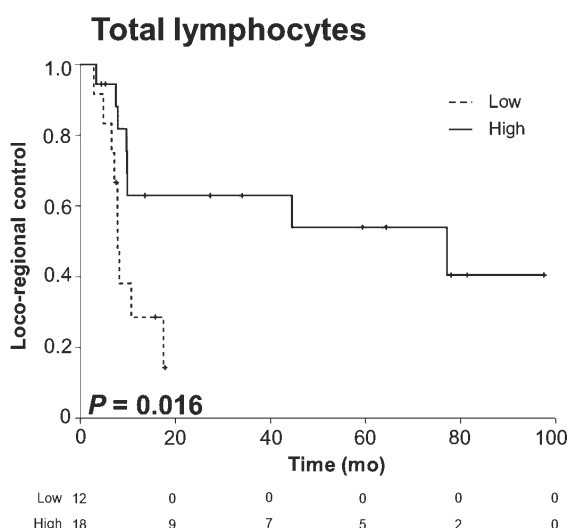
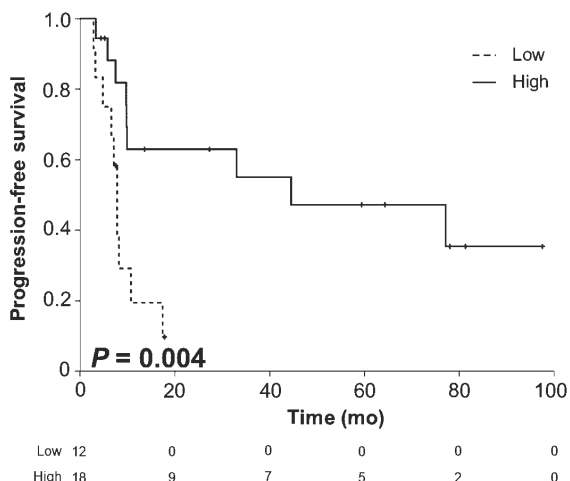
Figure 4. High lymphocyte levels determine the response of hypoxia-resolving and non-resolving HNSCCs to chemoradiation. Kaplan-Meier curves showing LRC (A) and PFS (B) depending on early hypoxia resolution and total tumor lymphocyte levels. LRC (C) and PFS (D) divided by early hypoxia resolution and CD3-positive lymphocyte levels.

Table 1: Patient/tumor characteristics.

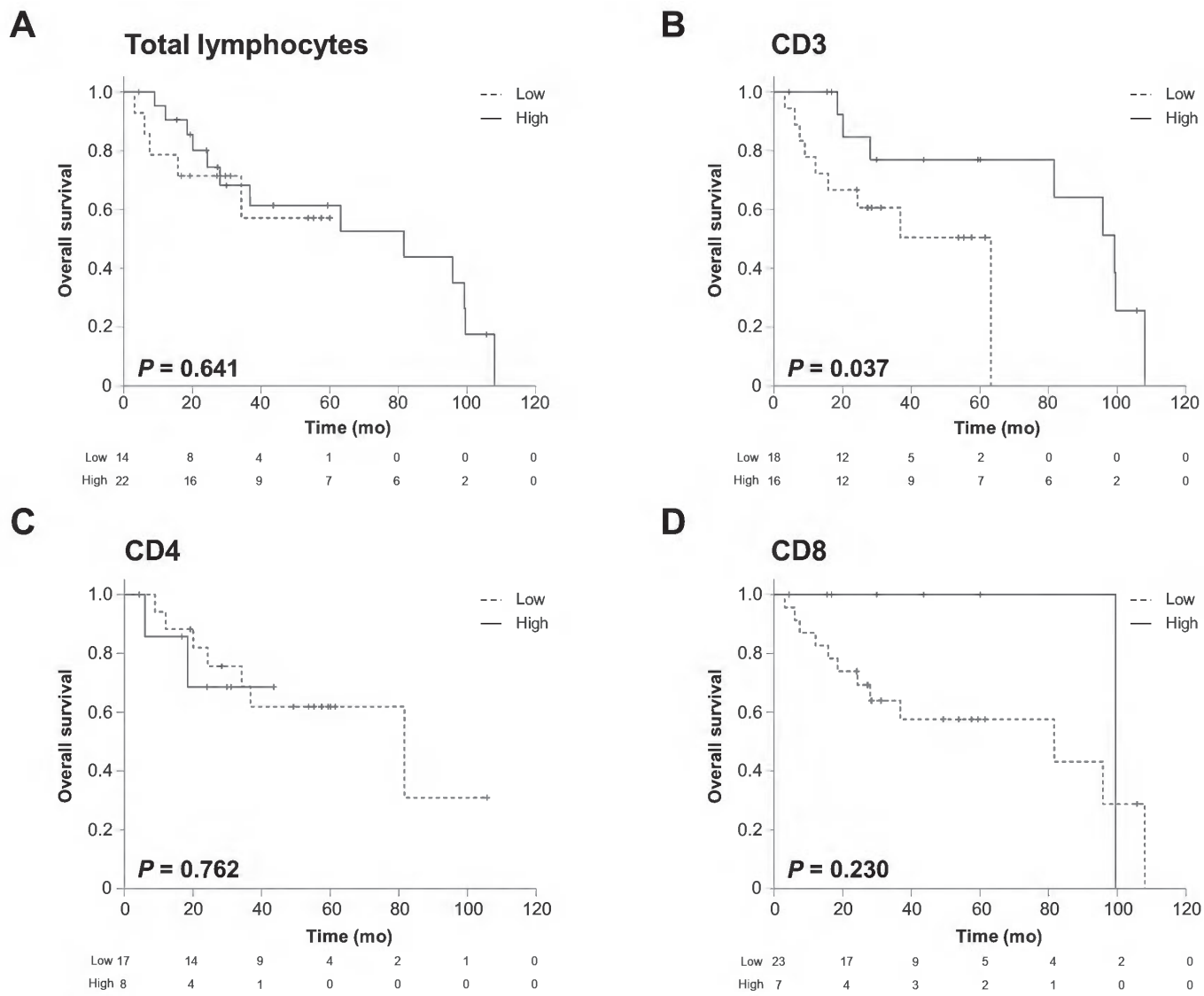
Tumor localization	n	%
Oral cavity	2	4.1
Oropharynx	19	38.8
Hypopharynx	12	24.5
Larynx	7	14.3
Multi-level	9	18.4
T stage		
T1	1	2.0
T2	4	8.2
T3	14	28.6
T4	30	61.2
N stage		
N0	4	8.2
N1	1	2.0
N2a	0	0.0
N2b	9	18.4
N2c	35	71.4
HPV		
HPV-positive	9	18.4
HPV-negative	40	81.6

Table 2: Pairwise correlations between immune biomarkers and tumor hypoxia. R and p values of Pearson correlations are indicated.

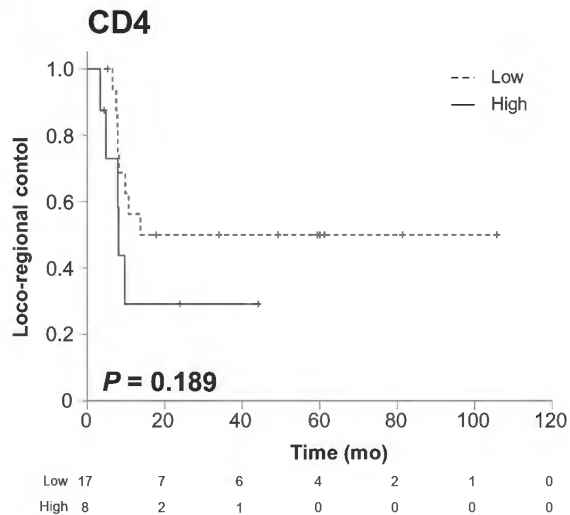
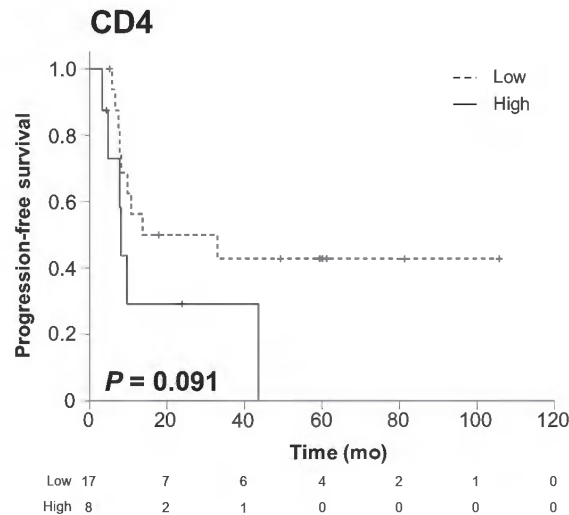
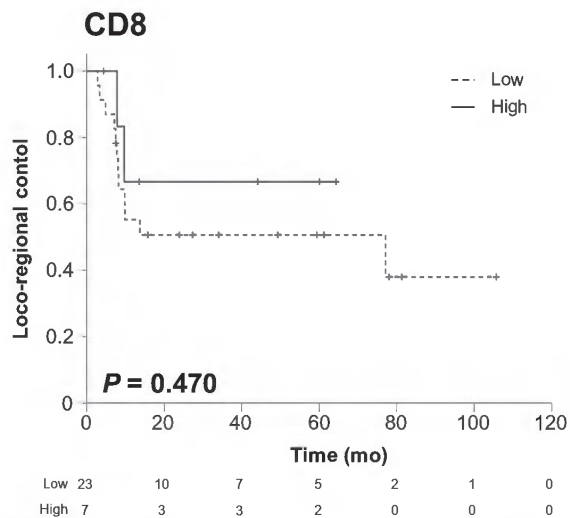
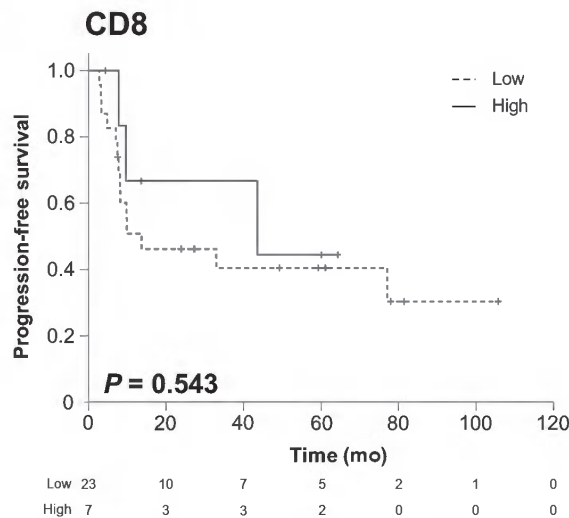
		tumor volume	hypoxic subvolume	SUV w0	SUV w2	SUV w5	Δ SUV w0-w2	Δ SUV w2-w5
lymphocytes	r	-0.247	-0.023	-0.033	0.008	0.018	0.061	0.002
	p	0.135	0.887	0.844	0.961	0.915	0.718	0.990
CD3	r	0.059	0.050	0.015	-0.007	0.233	-0.062	0.056
	p	0.728	0.770	0.931	0.968	0.184	0.724	0.753
CD4	r	0.303	-0.120	-0.092	-0.171	0.225	-0.093	0.145
	p	0.068	0.480	0.588	0.327	0.200	0.594	0.414
CD8	r	0.232	0.057	-0.116	-0.110	0.091	-0.010	0.137
	p	0.168	0.738	0.495	0.531	0.609	0.957	0.441

A**B****C****D**

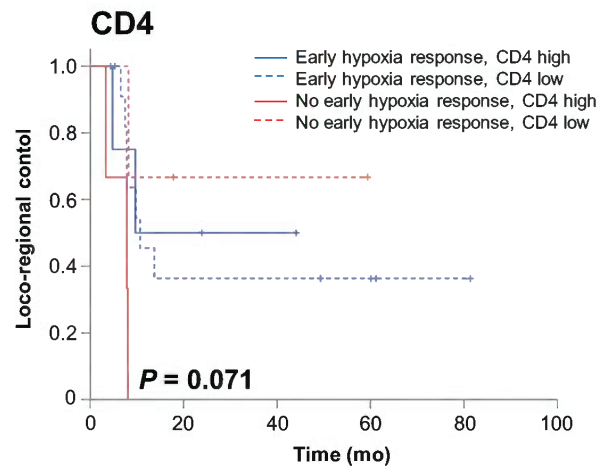
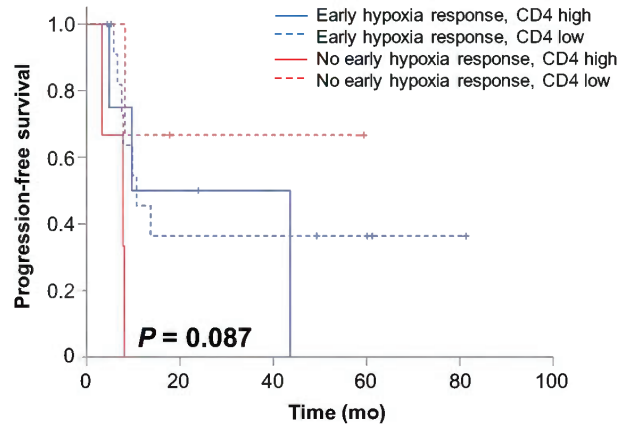
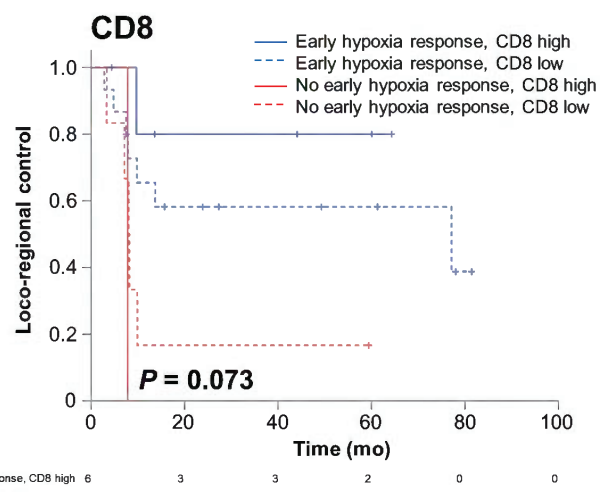
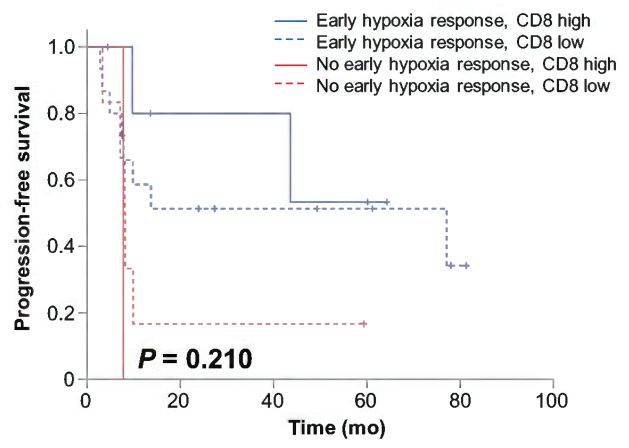
Supplementary figure 1. LRC and PFS of HPV-negative HNSCC patients depending on early hypoxia response and levels of tumor-infiltrating lymphocytes. Kaplan-Meier curves showing LRC (A) and PFS (B) depending on hypoxia response in weeks 2 of chemoradiation. LRC (C) and PFS (D) stratified by levels of tumor-infiltrating lymphocytes.



Supplementary figure 2. OS for HNSCC patients receiving definitive chemoradiation in dependence of their levels of infiltrating lymphocytes. Kaplan-Meier curves demonstrating OS depending on total lymphocyte (A), CD3-positive (B), CD4-positive (C) and CD8-positive lymphocyte levels in pre-therapeutic tumor biopsies. *P* values are obtained from log-rank tests testing for differences between the Kaplan-Meier curves.

A**B****C****D**

Supplementary figure 3. LRC and PFS as a function of CD4- and CD8-positive T lymphocytes. Kaplan-Meier curves demonstrating LRC and PFS depending on CD4-positive (**A and B**) and CD8-positive lymphocyte (**C and D**) levels. P values are obtained from log-rank tests testing for differences between the Kaplan-Meier curves.

A**B****C****D**

Supplementary figure 4. LRC and PFS of HNSCC patients depending on early hypoxia response and levels of CD4- and CD8-positive lymphocytes. Kaplan-Meier curves showing LRC (A) and PFS (B) depending on early hypoxia resolution and CD4-positive lymphocyte levels. LRC (C) and PFS (D) stratified by early hypoxia resolution and levels of CD8-positive lymphocytes.

Supplementary table 1: Description of antibodies used for immunohistochemical stains and corresponding antigen retrieval.

Antigen	Clone	Company	Dilution	Antigen retrieval
CD3	2GV6	Roche/Ventana	Prediluted	Citrate buffer pH 6,1
CD4	SP35	Roche/Ventana	Prediluted	Citrate buffer pH 9
CD8	SP57	Roche/Ventana	Prediluted	Tris-EDTA buffer pH 9
PD-1	NAT105	Roche/Ventana	Prediluted	Tris-EDTA buffer pH 9
PD-L1	SP263	Roche/Ventana	Prediluted	Tris-EDTA buffer pH 9
CAIX	C48E	Cell Signaling	1:300	pH 6.1 citrate buffer
CD34	QBEnd10 (IR632)	DAKO	Prediluted	pH 6.1 citrate buffer
CD44	156-3C11	Cell Signaling	1:500	pH 6.1 citrate buffer
HIF1α	MAB1935	R&D	1:100	pH 6.1 citrate buffer

Supplementary table 2: Pairwise correlations between immune and hypoxia biomarkers. Pearson correlations were conducted, and Pearson's r and p values are indicated in the table.

		HIF1α*	CAIX†	CD34
Lymphocytes	r	-0.034	0.074	0.476
	p	0.838	0.656	0.003 (*)
CD3	r	-0.300	0.234	0.313
	p	0.072	0.164	0.059
CD4	r	0.028	-0.048	0.181
	p	0.870	0.777	0.284
CD8	r	-0.323	0.196	0.275
	p	0.052	0.246	0.099

*HIF1α=Hypoxia-inducible factor-1α

†CAIX=Carbonic anhydrase IX

Supplementary table 3: Cox proportional hazards analyses of several tumor hypoxia-related parameters regarding their impact on LRC and PFS.

Univariate	LRC		PFS	
	HR	p-value	HR	p-value
Tumor hypoxic subvolume _{SUV=1.4} wk0 ≥ 3.87 mL (median)	0.533	0.152	0.560	0.159
Tumor hypoxic subvolume _{SUV=1.4} wk2 ≥ 0.02 mL (median)	1.502	0.343	1.391	0.421
Tumor hypoxic subvolume _{SUV=1.4} wk5 ≥ 0.00 mL (median)	0.942	0.937	0.783	0.743
SUV index wk0 (tumor-to-muscle) ≥ 1.89 (median)	1.243	0.612	1.520	0.312
SUV index wk2 (tumor-to-muscle) ≥ 1.51 (median)	1.883	0.158	1.702	0.213
SUV index wk5 (tumor-to-muscle) ≥ 1.31 (median)	0.715	0.460	0.450	0.725
SUV index wk0 (tumor-to-muscle) ≥ 1.4	0.849	0.791	1.058	0.927
SUV index wk0 (tumor-to-muscle) ≥ 1.6	0.950	0.914	1.169	0.738
SUV index wk2 (tumor-to-muscle) ≥ 1.4	3.189	0.041	3.661	0.021
SUV index wk2 (tumor-to-muscle) ≥ 1.6	1.580	0.296	1.463	0.363
SUV index wk5 (tumor-to-muscle) ≥ 1.4	0.904	0.839	0.752	0.553
SUV index wk5 (tumor-to-muscle) ≥ 1.6	1.902	0.311	1.685	0.409
ΔSUV index (tumor-to-muscle) wk0-2 ≥ 0	3.111	0.011	2.487	0.035
Δ SUV index (tumor-to-muscle) wk0-5 ≥ 0	1.126	0.793	0.863	0.731
Δ SUV index (tumor-to-muscle) wk2-5 ≥ 0	0.283	0.092	0.242	0.057